THE JOURNAL OF PHYSICAL CHEMISTRY Letters

pubs.acs.org/JPCL Letter

Intraband Relaxation Dynamics of Charge Carriers within CdTe Quantum Wires

William M. Sanderson, Fudong Wang, Joshua Schrier, William E. Buhro, and Richard A. Loomis*

Cite This: J. Phys. Chem. Lett. 2020, 11, 4901−4910 Read Online

ACCESS | Metrics & More | Article Recommendations | Supporting Information

ABSTRACT: The state-to-state intraband relaxation dynamics of charge carriers photogenerated within CdTe quantum wires (QWs) are characterized via transient absorption spectroscopy. Overlapping signals from the energetic-shifting of the quantum-confinement features and the occupancy of carriers in the states associated with these features are separated using the quantum-state renormalization model. Holes generated with an excitation energy of 2.75 eV reach the band edge within the instrument response of the measurement, ∼200 fs. This extremely short relaxation time is consistent with the low photoluminescence quantum yield of the QWs, ∼0.2%, and the presence of alternative relaxation pathways for the holes. The electrons relax through the different energetically available quantum-confinement states, likely via phonon coupling, with an overall rate of ∼0.6 eV ps^{-1}.

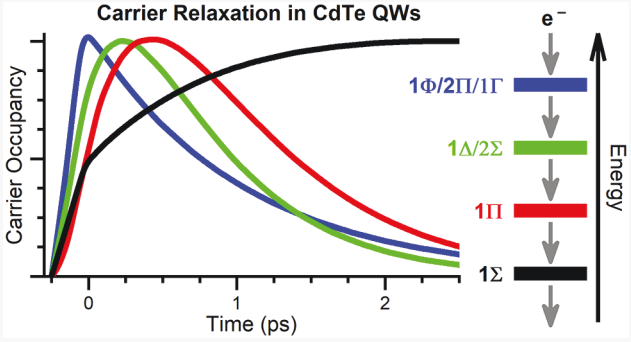

In photovoltaic devices it would be ideal that for every photon absorbed, at least one electron and one hole would be collected separately as electrical current with little or no loss of energy. Photovoltaic devices that incorporate semiconductor nanoparticles (NPs) as the absorbing medium offer large absorption cross sections and energetic tunability of absorbance and emission through size control of the semiconductor and resultant quantum-confinement.[1] An absorption event in a semiconductor NP promotes an electron to the conduction band (CB) and generates a hole, or an electron-deficient region, in the valence band (VB). These electrons and holes quickly relax through the manifold of CB and VB states to the lowest-energy states of the NP. Carriers at the band edge may recombine on a slower time scale via emission.

The intraband relaxation may occur via carrier coupling with phonons. The energy spacings between the quantum-confinement states in NPs, however, can be large, especially in the CB of zero-dimensional (0D) semiconductor quantum dots (QDs), and a "phonon bottleneck" can result.[2−9] As a result, electrons in QDs preferentially relax through an Auger mechanism, where the quantum-confinement kinetic energy of an electron transfers to a hole, re-exciting that hole in the VB.[10] The intraband relaxation dynamics (IRD) of the charge carriers can also be influenced by the surfaces of the NPs; dangling bonds, surface ligands, and possible shell materials can alter the energetics of the semiconductor NPs or relaxation pathways external to the NPs.[11−24] These competing pathways lead to an excitation energy dependence of the photoluminescence (PL) quantum yields of the NPs.[25−30]

The relaxation dynamics that occur within semiconductor NPs are commonly characterized using transient absorption (TA) spectroscopy to photoexcite the carriers and probe the changes in the absorption spectrum induced by the carriers.[3,5,10,18,31−42] These TA data are often complicated and difficult to analyze due to overlapping transient signals. In ref 43, we demonstrated that some of the overlapping induced-absorption (ΔAbs > 0) and bleach (ΔAbs < 0) signals within the TA data are associated with changes in the electron density distribution induced by photoexcitation; these effects are termed quantum-state renormalization (QSR).[43] In this Letter, we report on the IRD of photoexcited charge carriers within an ensemble of CdTe quantum wires (QWs) characterized using TA spectroscopy.[43] The densities of states within the CB and VB of one-dimensional (1D) quantum wires (QWs) contain a continuum associated with the translational motion of the charge carriers along the unconfined dimension. The IRD in these QWs are likely different than those in highly studied QDs, as discrete energetic jumps of the carriers between the quantum-confinement states are not strictly necessary. Because total momentum must be conserved, there are likely additional constraints governing the relaxation of the carriers in 1D QWs

Received: April 30, 2020
Accepted: June 3, 2020
Published: June 3, 2020

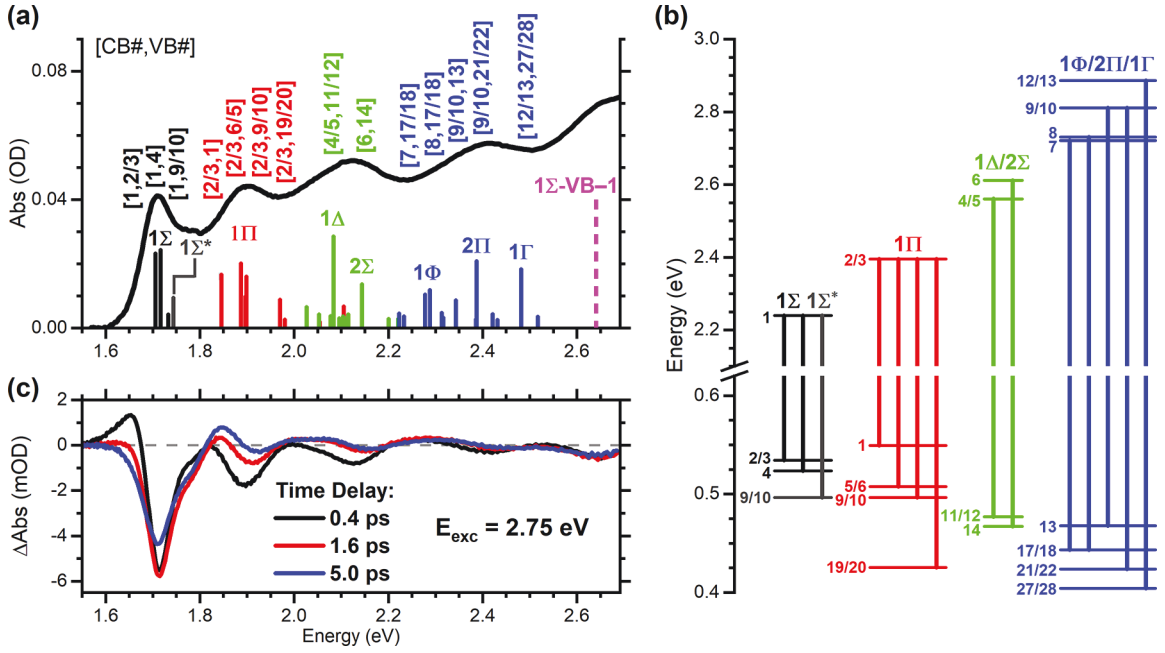

Figure 1. Spectra and energy level diagram of 7.5 nm CdTe QWs. (a) Abs(E) spectrum and prominent transitions (stick spectra) labeled with the indices of the electron and hole quantum-confinement states in the CB and VB using the notation [CB#,VB#]. The transitions are grouped together based on the CB states accessed, 1Σ, 1Π, 1Δ/2Σ, and 1Φ/2Π/1Γ, as illustrated in (b). The feature at ∼2.64 eV contains contributions from 1Σ-VB−1 transitions. (c) TA spectra recorded with E_{exc} = 2.75 eV at t = 0.4, 1.6, and 5.0 ps are plotted as black, red, and blue.

than in 0D QDs. We employed the QSR model[43] to analyze the TA data and to obtain the time-dependent carrier occupancies within the different spectral features. The temporal profiles of the occupancy features enabled the IRD of the charge carriers through the different sub-bands to be mapped with time.

Steady-State Optical Spectroscopy. The QSR model utilizes the steady-state absorption spectrum of an NP sample, $Abs_{ss}(E)$, to accurately account for the transitions and heterogeneities within the sample. For the sample of CdTe QWs, average diameter of 7.5(9) nm and lengths of 1−10 μm, the differences in morphologies could result in broadening of the spectral features. The $Abs_{ss}(E)$ spectrum includes these heterogeneities, and assumptions regarding sizes and the identification of specific transitions are not necessary. Note that the PL spectra recorded for single CdTe QWs with similar physical characteristics as those investigated here were nearly identical with approximately the same center energies and breadths.[44]

The steady-state absorption spectrum, $Abs_{ss}(E)$, of the sample of the CdTe QWs suspended in dried toluene is plotted in Figure 1a. Five prominent peaks and one weak peak, at ∼1.78 eV, were identified in the spectrum; the peak energies are listed in Supporting Information Table S1. The PL spectrum of the CdTe QWs, Figure S4, has a maximum near 1.69 eV, or ∼17 meV below the lowest-energy absorption feature. Typical of as-synthesized CdTe QW samples, these CdTe QWs exhibited a low PL quantum yield (Φ_{PL}) of ∼0.20(3)% measured using an excitation energy of E_{exc} = 2.76 eV. The low Φ_{PL} of the sample indicates a majority of photogenerated charge carriers access nonradiative pathways during intraband relaxation within the CB and VB or at the band edge.

Quantum-Confinement States and Transitions. The quantum-confinement states in the VB and CB of the CdTe QWs and the corresponding transition energies and strengths were calculated to identify the contributions within the spectral data. The energies of the most intense transitions are included in Figure 1a as vertical lines with heights depicting the relative transition strengths. The transition probabilities were computed from the wave functions of each state using eq S2 in the Supporting Information, Section 2. The indices of the electron (CB#) and hole (VB#) quantum-confinement states are listed above each line using the notation [CB#,VB#]. The energy-state diagram in Figure 1b includes the prominent transitions and the states likely involved. The calculations indicate the spacings between the absorption features are largely dictated by the energies of the quantum-confinement states in the CB.[45] The mixed nature of the quantum-confinement states in the VB gives rise to the large number of transitions and the breadths of the features.[45] Consequently, we label each spectral feature with the quantum-confinement state(s) in the CB accessed by the transitions that lie within that feature.

The transitions involving the lowest-energy quantum-confinement states in the VB are the [2/3,1] lines, and they are within the 1Π absorption feature. On the other hand, the lowest-energy $1\Sigma_e$ state in the CB is accessed by transitions that include numerous higher-energy VB states. Based on the energetic ordering of the transitions, we associate the [1,2/3] and [1,4] lines with the 1Σ feature and the [1,9/10] line with the weak 1Σ* absorption feature at slightly higher energies. The absorption feature at ∼2.64 eV is energetically separated from the band edge transitions by ∼0.94 eV. This value is approximately the energetic difference between VB (Γ_8) and VB−1 (Γ_7) band of bulk CdTe, ∼0.9 eV,[46] and we assign it accordingly to 1Σ-VB−1 transitions. It is likely there are other transitions within this spectral feature, such as transitions from the VB to higher-energy states in the CB, e.g. 1H, 2Δ, and 1I. These assignments suggest photogenerated holes that achieve a thermal equilibrium in the quantum-confinement states near

https://dx.doi.org/10.1021/acs.jpclett.0c01326
J. Phys. Chem. Lett. 2020, 11, 4901−4910

the band edge would contribute to the occupancy signals in the 1Π feature as well as in the 1Σ feature in the TA data. In contrast, electrons in the $1\Sigma_e$ state would result in TA signals in the 1Σ, 1Σ*, and 1Σ-VB−1 features.

Transient Absorption Spectroscopy. TA experiments were performed on the CdTe QWs using E_{exc} = 2.75 and 2.26 eV to prepare the electrons and holes with different excess kinetic energies. Unless otherwise stated, the excitation fluences were kept low, 9.7 μJ cm^{-2} pulse^{-1} (E_{exc} = 2.75 eV) and 11.3 μJ cm^{-2} pulse^{-1} (E_{exc} = 2.26 eV), to minimize the average number of carriers excited in the QWs, ⟨N⟩. Estimates for ⟨N⟩ are ∼74 and ∼63 excitons μm^{-1} pulse^{-1} for E_{exc} = 2.75 and 2.26 eV, and no multibody effects were observed with fluences <20 μJ cm^{-2} pulse^{-1}. See Supporting Information Section 3 for details regarding ⟨N⟩ estimates and for a comparison of the 1Σ temporal profiles recorded at multiple excitation fluences. The TA spectra, $\Delta Abs_{TA}(E, t)$, acquired at three time delays, t, and E_{exc} = 2.75 eV are plotted in Figure 1c. As is typical for TA spectra of NPs, these spectra are complicated with overlapping induced-absorption (ΔAbs > 0) and bleach (ΔAbs < 0) signals.

Quantum-State Renormalization. The QSR model was presented and implemented on the CdTe QW TA spectra collected with E_{exc} = 2.75 eV in ref 43. The contributions from QSR in the TA spectra were determined at each time t by taking the difference between the absorption spectrum shifted by an amount $\Delta E_{QSR}(t)$ and the $Abs_{ss}(E)$ spectrum:

$$\Delta Abs_{QSR}(E, t) = C(t)[Abs(E - \Delta E_{QSR}(t)) - Abs_{ss}(E)] \quad (1)$$

where $C(t)$ is a scaling factor proportional to the population of the carriers in the QWs. Eq 1 was fit to the TA spectrum at each t, $\Delta Abs_{TA}(E, t)$, using $C(t)$ and $\Delta E_{QSR}(t)$ as fitting parameters as described in the Supporting Information. The fitting procedure yielded population values, $C(t)$, and a universal QSR shift, $\Delta E_{QSR}(t)$ = 13(1) meV, which in turn permitted the contributions from QSR, $\Delta Abs_{QSR}(E, t)$, to be identified at each t.[43] The fit for the t = 35 ps data is illustrated in Figure 2a. The difference between the $\Delta Abs_{QSR}(E, t)$ spectrum and the TA spectrum, $\Delta Abs_{TA}(E, t)$, at each t yields the occupancy spectrum, $\Delta Abs_{Occ}(E, t)$. The $\Delta Abs_{Occ}(E, t)$ spectra obtained for t = 0.6, 1.4, and 35 ps are graphed in Figure 2b. All of the $\Delta Abs_{Occ}(E, t)$ spectra for $t \leq 4$ ps are included in the 2D color-contour plot in Figure 2c, and the full data set extends out to $t > 7$ ns. These spectra contain features associated with the occupancy of charge carriers in the QSR-shifted quantum-confinement states, and these shifted features are labeled with primes, e.g., 1Σ′, 1Σ*′, 1Π′, 1Δ′/2Σ′, etc. The TA data collected with E_{exc} = 2.26 eV were also analyzed, and a universal QSR shift of $\Delta E_{QSR}(t)$ = 12(2) meV was determined. Additional details for these data, the fitting procedure, and the results are provided in Supporting Information Section 5.

The $\Delta Abs_{Occ}(E, t)$ data in Figure 2 (E_{exc} = 2.75 eV) and in Figure S8 (E_{exc} = 2.26 eV) indicate several key results. (1) Carriers occupy states in all of the features observed in the $Abs(E)$ spectrum at short t. (2) The occupancy features at lower energies have slower growths and decays than those at higher energies, likely due to the relaxation of the carriers from higher- to lower-lying states. The exception to this trend is the 1Σ′-VB−1′ feature, as it grows in and decays away in a similar manner as the 1Σ′ occupancy feature. (3) For $t \geq 4$ ps, the only features with measurable occupancies are the 1Σ′, 1Σ*′, and the higher-energy 1Σ′-VB−1′ features. (4) Nearly identical universal QSR shifts of $\Delta E_{QSR}(t)$ = 13(1) and 12(2) meV were determined in the fitting of the E_{exc} = 2.75 and 2.26 eV TA data at long t, when carriers are presumably in the lowest-energy quantum-confinement states of the CB and VB. (5) Each of the occupancy features shift by additional, independent amounts, especially at short t.

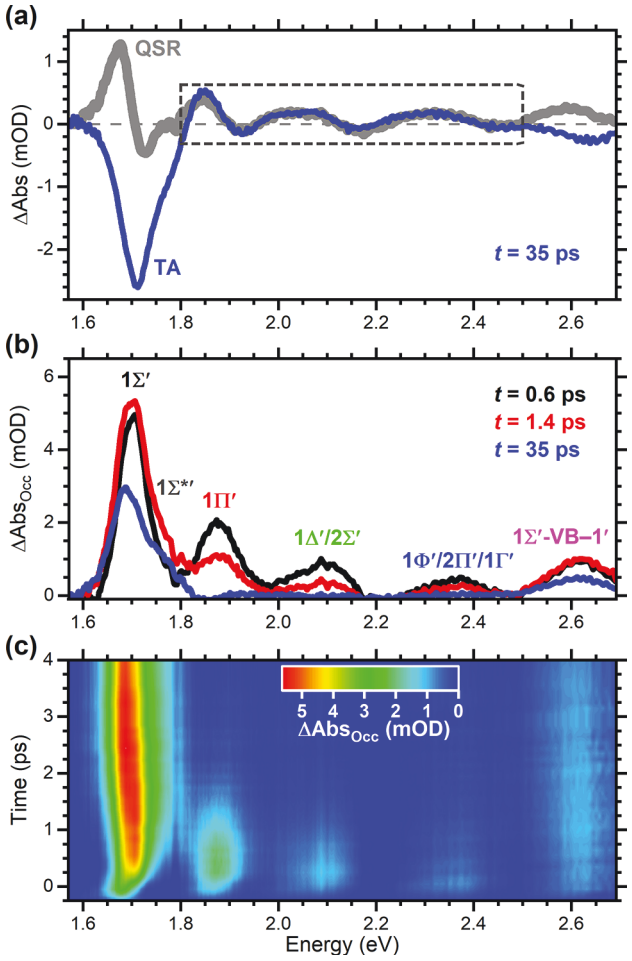

Figure 2. QSR, TA, and occupancy spectra for excitation with 2.75 eV. (a) The TA spectrum at t = 35 ps (blue) is overlaid with the QSR spectrum (gray) obtained by fitting the region shown (inset). (b) The $\Delta Abs_{Occ}(E, t)$ spectra, obtained for three time delays, are plotted with the features labeled. (c) 2D color-contour plot of the $\Delta Abs_{Occ}(E, t)$ spectra for $t \leq 4$ ps.

Carrier Occupancies and Dynamics. The occupancies of charge carriers within the spectral features were quantified by fitting the $\Delta Abs_{Occ}(E, t)$ spectrum at each t to a sum of Gaussian peaks using the amplitudes, center energies, and widths as parameters. Examples of fits are included in Figures S9 and S10. The integrated area of each Gaussian peak is proportional to the occupancies of charge carriers in the quantum-confinement states accessed by transitions within that feature at that t. A plot of the integrated area of each peak versus t yields the temporal profile of the carrier occupancies in those features, as shown in Figure 3. The temporal profile of each occupancy feature was fit to a sum of exponential rises and decays convoluted with a 200 fs Gaussian instrument response function (IRF), as described and summarized in Supporting Information Section 7. The rise and decay constants, τ_r and τ_d, obtained for the occupancy profiles are included in Table 1.

https://dx.doi.org/10.1021/acs.jpclett.0c01326
J. Phys. Chem. Lett. 2020, 11, 4901−4910

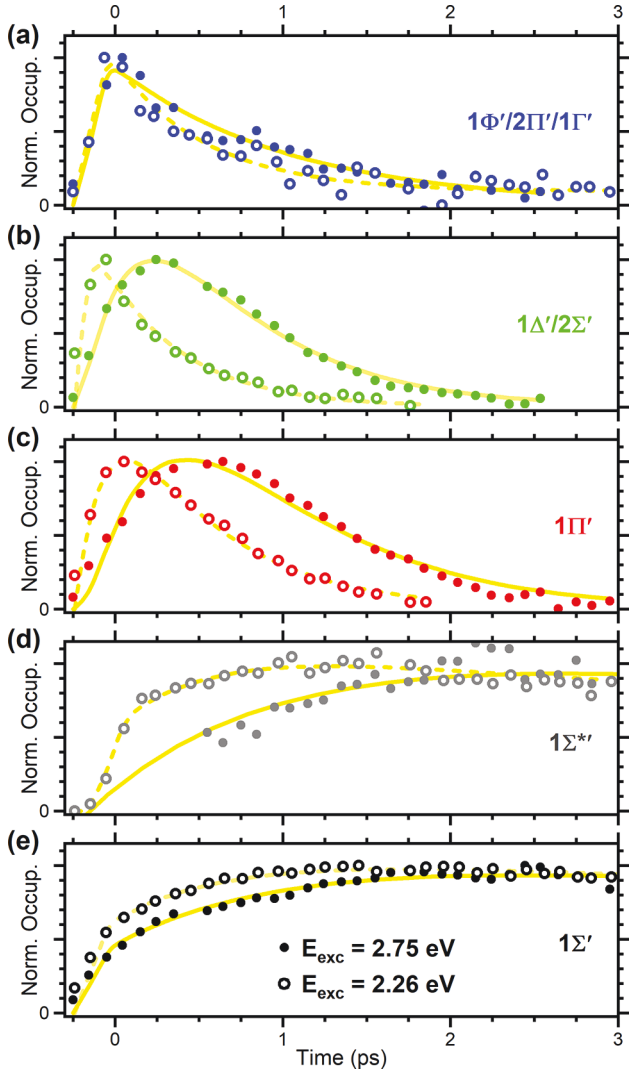

Figure 3. Occupancies plotted versus time. The occupancy profiles for the features (a) 1Φ′/2Π′/1Γ′, (b) 1Δ′/2Σ′, (c) 1Π′, (d) 1Σ*′, and (e) 1Σ′ obtained for E_{exc} = 2.75 and 2.26 eV are shown as filled and open symbols, respectively. Each profile was fit to a sum of exponential rises and decays (lines).

Table 1. Lifetimes of the Occupancy Profiles

	E_{exc}= 2.26 eV		E_{exc}= 2.75 eV	
Quantum States	τ_r (ps)	τ_d (ps)	τ_r (ps)	τ_d (ps)
1Σ′	0.66(1)[b]	249(2)[a]	1.10(2)[b]	232(6)[a]
1Σ*′	0.63(3)[b]	250(20)[a]	1.3(3)[c]	230(30)[a]
1Π′	IRF	0.60(5)	0.50(2)	0.65(2)
1Δ′/2Σ′	IRF	0.47(8)	0.29(1)	0.62(2)
1Φ′/2Π′/1Γ′	IRF[d]	0.54(4)[d]	IRF	1.03(6)

[a]Contained a sum of four decays, and values are average lifetimes. [b]Was best fit with one component within the IRF and a second component with the lifetime indicated. [c]Only points for t > 0.60 ps were available for fitting. [d]Included a vertical offset in the fitting.

The time constants of each profile collected with E_{exc} = 2.75 eV are longer than those collected with E_{exc} = 2.26 eV. This is consistent with the preparation of the electrons and holes to higher energies above the band edge, and the longer times necessary to reach and relax out of these states. Using the calculated transitions as a guide, E_{exc} = 2.75 eV results in the electrons and holes being prepared with ∼0.65 and ∼0.42 eV above the lowest-energy quantum confinement states in the CB and VB, respectively. For E_{exc} = 2.26 eV the electrons and holes are prepared with ∼0.48 and ∼0.12 eV of excess energy. In addition, the occupancies in the higher-energy features grow in faster than in the lower-energy features, $\tau_r(1\Phi'/2\Pi'/1\Gamma') \leq \tau_r(1\Delta'/2\Sigma') \leq \tau_r(1\Pi') \leq \tau_r(1\Sigma' \text{ or } 1\Sigma^{*\prime})$, for both excitation energies. This suggests the carriers are relaxing sequentially through the states energetically available until they reach the states near the band edge. The major exception to this trend is the occupancy profile of the 1Σ′-VB−1′ feature. As mentioned, this feature likely includes overlapping contributions from transitions between the VB and high-energy quantum-confinement states in the CB and transitions between states in the VB−1′ and the $1\Sigma_e'$ state. Note that significantly different profiles would be obtained if the temporal profiles of the $\Delta Abs_{TA}(E, t)$ data at the energies of the different spectral features were used instead of the profiles of the occupancy features obtained using the QSR model, as illustrated in Supporting Information Section 8.

Separation of Electron and Hole Dynamics. Scrutiny of the occupancy data enables the relaxation dynamics of the electrons to be separated from those of the holes. As already described, the 1Σ′, 1Σ*′, and 1Σ′-VB−1′ features are attributed to transitions from different states in the VB to the same $1\Sigma_e$ state in the CB. The temporal profiles of the 1Σ′, 1Σ*′, and 1Σ′-VB−1′ features collected with E_{exc} = 2.75 and 2.26 eV are plotted in Figure 4 and Figure S12, respectively, as

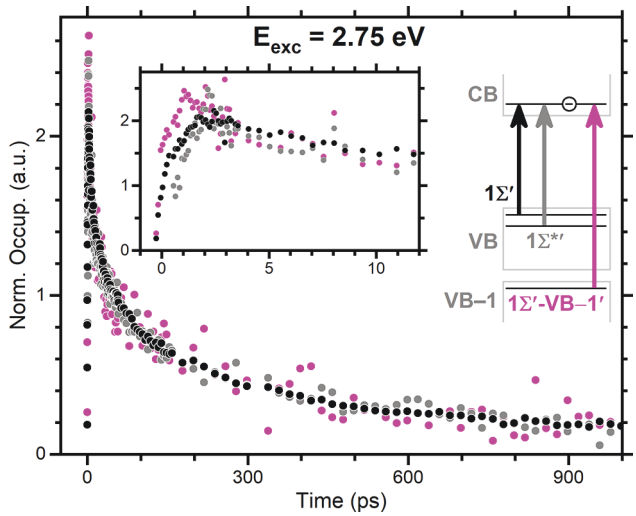

Figure 4. Occupancy profiles of the 1Σ′, 1Σ*′, and 1Σ′-VB−1′ features acquired with E_{exc} = 2.75 eV are plotted as black, gray, and magenta symbols. Each profile is normalized to unity at t = 50 ps. Inset: short-time region. A schematic of the dominant transitions associated with each occupancy feature is also included.

black, gray, and magenta symbols. These profiles decay proportionally to each other, and there are only small differences present at the shortest times when contributions from holes may contribute. Thus, the long-time dynamics measurable in these TA experiments are associated with the occupancy of electrons in the $1\Sigma_e'$ state. The measured decay constants span three orders of magnitude in time, and the decay profiles are proportional to the photoluminescence decay profiles reported previously[47] and plotted in Figure S7. The time constants obtained from fitting the 1Σ′ and 1Σ*′

https://dx.doi.org/10.1021/acs.jpclett.0c01326
J. Phys. Chem. Lett. 2020, 11, 4901−4910

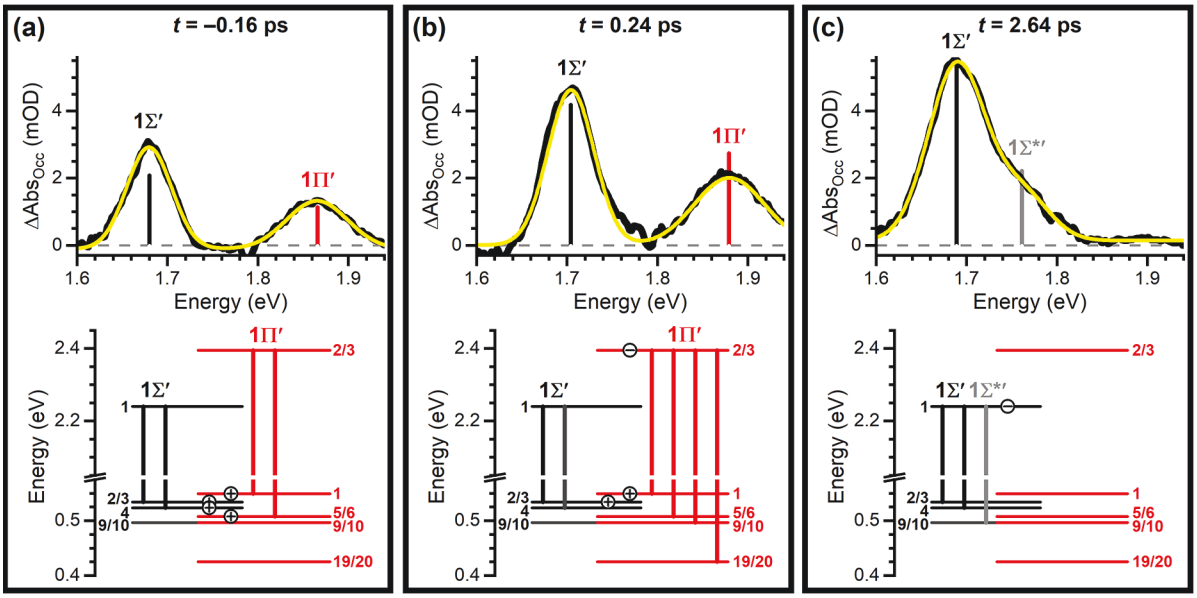

Figure 5. Carrier occupancy near the band edge (E_{exc} = 2.75 eV) recorded at (a) t = −0.16 ps, (b) t = 0.24 ps, and (c) t = 2.64 ps. The $\Delta Abs_{Occ}(E, t)$ spectra were fit to a sum of Gaussians (yellow), and the integrated intensities of the 1Σ′, 1Σ*′, and 1Π′ features are indicated by the solid lines. Schematics of the states and transitions giving rise to the observed occupancies are shown at the bottom.

temporal profiles, Table S3 and Table S4, are typical of NP samples with low Φ_{PL} values and large contributions from nonradiative pathways.

Additional insights into the IRD are gained through inspection of the lowest-energy region of the occupancy spectra, $\Delta Abs_{Occ}(E, t)$. Occupancy spectra recorded at three different t with E_{exc} = 2.75 eV are included in Figure 5. The spectra were fit to a sum of Gaussian peaks, and the integrated intensities of the peaks are shown as vertical lines. At the earliest times during the excitation pulse, $\Delta Abs_{Occ}(E, -0.16$ ps), there were discernible occupancies only in the 1Σ′ and 1Π′ features and none in the 1Σ*′ feature. Recall, the 1Σ*′ feature is a direct signature of electrons populating the $1\Sigma_e'$ (CB1) quantum-confinement state. Thus, most of these occupancy signals in this energy region and t are attributed to holes that relaxed very quickly down to the low-lying quantum states, as depicted in the energy-level diagram at the bottom of Figure 5a. The occupancies in the 1Σ′ and 1Π′ features increased just after the excitation pulse, $\Delta Abs_{Occ}(E,$ 0.24 ps) in Figure 5b. These growths are attributed to the continued relaxation of the holes to the few lowest-energy states in the VB and electrons into the CB2/3 state. Because there are no identifiable signals in the 1Σ*′ feature, there were a negligible number of electrons present in the lowest-energy CB1 state at this t. At slightly longer delays after photoexcitation, t = 2.64 ps, there are no detectable signals in the higher-energy occupancy features, with the exception of the 1Σ′-VB−1′ feature. In the lower-energy region, Figure 5c, occupancies only in the 1Σ′ and energetically overlapping 1Σ*′ feature are measurable. The 1Σ*′ occupancy signal provides evidence for electrons reaching the $1\Sigma_e'$ (CB1) quantum-confinement state. Because there is very little or no signal in the 1Π′ feature, there was no discernible hole occupancy in the VB1 state by this t. We presume a majority of the holes near the band edge either recombined radiatively or became trapped outside of the CdTe QWs, and the relaxing electrons in the $1\Sigma_e'$ state were in excess by these longer times.

The TA and occupancy data in this spectral region recorded with E_{exc} = 2.26 eV reveal similar electron and hole dynamics, although the time scales for relaxing to the band edge are shorter. The occupancy spectrum recorded at t = 0.24 ps, Figure S13a, contains signals not only in both the 1Σ′ and 1Π′ features, but also a weak signal in the 1Σ*′ feature. This indicates there were electrons and holes populating the lowest-energy CB1 and VB1 quantum-confinement states just after excitation. By t = 2.64 ps, the amplitude of the 1Π′ feature is no longer discernible, and both the 1Σ′ and 1Σ*′ features reached their maximum amplitudes, Figure S13b. Once again, these occupancy signals suggest there was an excess of electrons present in the QWs in the CB1 state and negligible holes in the VB states by this t.

Intraband Relaxation. The comparisons of the occupancy signals enabled the contributions from the electrons and holes to be identified. After photoexcitation, the prepared electron and holes promptly relaxed within the IRF of the TA experiments through the highly excited quantum-confinement states detected within the 1Φ′/2Π′/1Γ′ occupancy feature. The electrons and holes continued to relax through the lower-lying states and features until they reached the band edge, likely with dissimilar rates, or until they became trapped. The actual dynamics incurred by the charge carriers while undergoing intraband relaxation are much more complicated than suggested by the lifetimes included in Table 1. The measured rate for the growth of the 1Δ′/2Σ′ profile, $(0.29$ ps$)^{-1}$ for E_{exc} = 2.75 eV, is much faster than the decay of the next higher-energy 1Φ′/2Π′/1Γ′ profile, $(1.03$ ps$)^{-1}$. Similarly, the growth rate of the 1Π′ feature, $(0.50$ ps$)^{-1}$, is faster than the decay rate of the 1Δ′/2Σ′ feature, $(0.62$ ps$)^{-1}$. The kinetics of the 1Σ*′ and 1Σ′ occupancy features are even more complicated; the rise of the 1Σ′ feature grows in with a sum of two exponential terms and decays with a sum of four exponential decays. We unsuccessfully attempted to numerically model the carrier IRD in the CdTe QWs using the measured time constants, Tables S3 and S4, and including dissimilar relaxation rates for the electrons and holes for each

https://dx.doi.org/10.1021/acs.jpclett.0c01326
J. Phys. Chem. Lett. 2020, 11, 4901−4910

occupancy feature. Additional modeling attempts were made that included variable trapping rates. These efforts were also not successful in fitting the kinetics of the occupancy features without over-parametrizing the terms utilized.

There are several contributions in the IRD of the photoexcited charge carriers that could contribute to the occupancy data and that were likely not properly accounted for in the modeling. Each feature does not contain a single transition. The $1\Delta'/2\Sigma'$ feature, for instance, contains the two prominent transitions indicated in Figure 1b, and their transition strengths are not the same. Furthermore, the transitions within each feature are associated with a few states or even just a single state in the CB, but numerous states in the VB. The results presented in the previous section indicate the holes either became relaxed to the lowest-energy quantum-confinement states within the VB or became trapped on very fast time scales. In contrast, the electrons relax to the band edge on slower time scales, even though they sample fewer states. We recently characterized the excitation energy dependence of the Φ_{PL} of CdTe QWs, and the efficiency for carrier relaxation to the band edge is not unity, and there are competing pathways for carrier relaxation.[48] It is likely that the closely spaced quantum-confinement states in the VB, the continuum of states associated with each state, and the nonradiative relaxation pathways all contribute to the fast IRD of the holes. By comparison, the larger energetic spacings between the states in the CB and fewer nonradiative relaxation pathways may contribute to the slower relaxation of the electrons than the holes in these CdTe QWs. The temporary trapping of electrons during their relaxation to the band edge can also result in delayed relaxation to the band edge and extended carrier lifetimes.[49−52] As a result, there are additional steps and rates than those identifiable in the TA spectra, and more complicated relaxation schemes would be necessary to model the carrier dynamics.

The occupancy profiles of the features near the band edge do provide insight into the overall relaxation rates of the electrons and holes. The temporal profile of the integrated area of the $1\Sigma'$ feature collected with E_{exc} = 2.75 eV, plotted in Figure 3e, was fit to a sum of two exponential rises, and an instrument-limited component of ∼200 fs and a lifetime of 1.10(2) ps was obtained. The fast component was attributed to the relaxation of the holes to the VB2/3 and VB4 states near the band edge, and the slower component to the relaxation of the electrons to the lowest-energy $1\Sigma_e'$, CB1, state. Based on the calculations, we estimate E_{exc} = 2.75 eV promotes electron to ∼0.65 eV above the $1\Sigma_e'$ state. This energy combined with the 1.10 ps rise-time component of the $1\Sigma'$ occupancy profile yields an estimate of ∼0.6 eV ps^{-1} for the overall electron relaxation rate for E_{exc} = 2.75 eV. In comparison, the hole was prepared with ∼0.42 eV of excess energy, and the rise component is instrument limited, < 200 fs. Thus, only a lower limit of 2 eV ps^{-1} for the overall hole relaxation rate can be set. The fitting of the $1\Sigma'$ occupancy profile collected with E_{exc} = 2.26 eV yielded a slow component of 0.66(1) ps, and the fast component was instrument limited. This lower-energy excitation prepared the electrons and holes with ∼0.48 and ∼0.12 eV of excess energy, respectively. From these data, the overall electron relaxation rate for E_{exc} = 2.26 eV is estimated to be slightly higher, ∼0.7 eV ps^{-1}, and a lower limit of 0.6 eV ps^{-1} is set for the hole.

Studies of the carrier IRD within semiconductor QDs have shown that the large spacing between quantum-confinement states results in relaxation through a two-body Auger relaxation mechanism. The overall rate for electron relaxation to the band edge was estimated to be 1.2 eV ps^{-1} in CdSe QDs.[53] This two-body, Auger mechanism couples the kinetic energy of an excited electron to that of a hole. In the case of the CdTe QWs, the low Φ_{PL} of the sample, ∼0.2%, and the absence of hole occupancy signals within the $1\Pi'$ feature at $t \geq 2.64$ ps suggest there was not a large excess of holes present with which the electrons could couple. Furthermore, the measured overall rates of hole relaxation were determined to be notably higher than those of the electrons, and there were no delayed occupancy signals that could be associated with re-excitation of the holes. As a result, we deduce that two-body Auger relaxation is not a prominent relaxation mechanism in these CdTe QWs. Instead, we conclude the electrons and holes relax to the band edge via efficient phonon coupling and by accessing the continua of states above each quantum-confinement state. The relaxation rates measured for the electrons in these CdTe QWs, ∼0.6 and ∼0.7 eV ps^{-1}, are near the range of the rates for electron-LO phonon scattering relaxation in bulk CdSe, 0.2−0.5 eV ps^{-1}.[53] Following this comparison, we propose the slightly slower electron relaxation rate estimated for E_{exc} = 2.75 eV in comparison to that for E_{exc} = 2.26 eV is due to increased temperatures and phonon excitation within the QWs associated with the excess energies with which the charge carriers were prepared. The electron relaxation may also be slowed or delayed by becoming temporarily localized in shallow potential traps.[49−52]

Transient QSR during IRD. Within the QSR model, a universal $\Delta E_{QSR}(t)$ value of 13(1) meV with E_{exc} = 2.75 eV was determined from fitting the higher-energy features in the $\Delta Abs_{TA}(E, t)$ spectra with $t \geq 5$ ps. There is, however, no *a priori* reason that all of the quantum-confinement states and occupancy features should shift by the same $\Delta E_{QSR}(t)$ value after photoexcitation, especially at short t, when there are carriers within the manifold of higher-energy quantum-confinement states in the CB and VB states. Any additional shifting due to QSR or occupancy of electrons or holes in the individual quantum-confinement states at a given t would appear in the $\Delta Abs_{Occ}(E, t)$ spectra. The peak energies of the occupancy features are plotted relative to those measured in the steady-state $Abs(E)$ spectrum in Figure 6, and these short time windows emphasize the transient QSR, $\Delta E_{Occ}(t)$ that can occur.

The $\Delta E_{Occ}(t)$ of the lowest-energy $1\Sigma'$ feature obtained with E_{exc} = 2.75 and 2.26 eV are plotted as filled and open circles in Figure 6a. When exciting with 2.75 eV photons, the $1\Sigma'$ feature is shifted by nearly 30 meV at the shortest t, and it shifts to nearly 0 meV within 0.5 ps. The $1\Sigma'$ energy then increases again on a longer time scale to $\Delta E_{Occ}(t) \sim 17$ meV. This $\Delta E_{Occ}(t)$ value is slightly more than the universal shift of 13 meV, which was obtained by fitting several of the higher-energy features at the longest time delays. This long-time shift of the $1\Sigma'$ occupancy feature, 17 meV, was shown to give rise to the measured Stokes shift of the PL in these QWs.[43] The evolution of the $1\Sigma'$ feature measured with E_{exc} = 2.26 eV is similar, although the range of the peak energies is smaller and the time scales are shorter by ∼0.5 ps. These shorter time scales are consistent with the preparation of the carriers closer in energy to the band-edge states. The smaller shifting of the features measured at short t in the E_{exc} = 2.26 eV data indicate the QSR is higher when the carriers are occupying higher-energy states.

https://dx.doi.org/10.1021/acs.jpclett.0c01326
J. Phys. Chem. Lett. 2020, 11, 4901−4910

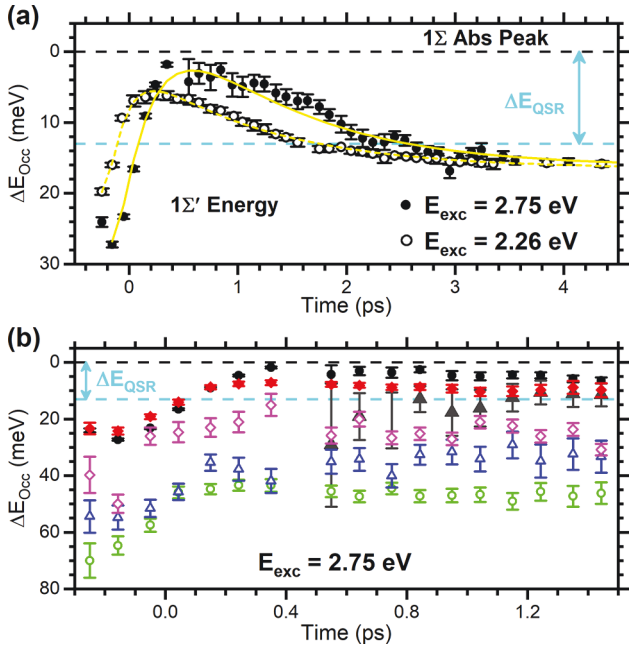

Figure 6. Time-resolved QSR. (a) The peak energy of the 1Σ′ feature obtained with E_{exc} = 2.75 eV (filled symbols) and 2.26 eV (open symbols) is plotted versus time. ΔE_{Occ} = 0 meV is the peak of the 1Σ absorption feature, and the universal QSR shift of 13 meV is indicated (cyan dashed line). Fits of the data to a sum of a single-exponential rise and decay (yellow) are included. (b) The energetic shifting of all of the features (E_{exc} = 2.75 eV) are plotted versus time. The energies of the peaks of the 1Σ′ (black), 1Σ*′ (gray), 1Π′ (red), 1Δ′/2Σ′ (green), 1Φ′/2Π′/1Γ′ (blue), and 1Σ′-VB−1′ (magenta, open) features are plotted relative to the energy of the corresponding feature in the steady-state Abs(E) spectrum. Note that the time scales of (a) and (b) are different.

After photoexcitation, the fraction of holes that did not become trapped during relaxation should have promptly reached a thermal distribution within the lowest-energy VB1, VB2/3, and VB4 states. The calculations, Table S2, indicate the VB2/3 states are ∼10 meV to lower energy than the VB4 state. Thus, the population of holes in the VB2/3 states should have been significantly higher, and the [1,2/3] transition should have been the major contributor to the 1Σ′ occupancy feature. The center energy of the 1Σ′ occupancy feature measured using E_{exc} = 2.75 eV is 1.673 eV at this short t. This energy is ∼30 meV below the calculated [1,2/3] absorption transition energy. This energy difference is associated with the QSR of the CB1 and VB2/3 states at the shortest t, when the holes were in the lowest-energy states, and the electrons were still in higher-energy states. At longer t, the transient QSR of these and all of the states should depend on the electron densities within the QWs as the electrons continued to relax and on the changing electron and hole populations.

The numerous transitions within each occupancy feature and the changing populations of the carriers in the states associated with these transitions can also give rise to amplitude modulations and a temporal evolution of the shapes and $\Delta E_{Occ}(t)$ values of the occupancy features. This behavior is observed in the temporal evolution of the 1Σ′ occupancy feature. As just discussed, the 1Σ′ occupancy feature at short t is dominated by holes in the VB2/3 states and the [1,2/3] transition. As the electrons begin to reach the $1\Sigma_e'$ state, all of the transitions within the 1Σ′ feature become bleached, and the energy of the feature shifts to smaller values due to contributions from other transitions, including the [1,4] transitions. The increasing breadth of the 1Σ′ feature with t, shown in Figure S14, reflects these changing contributions of the electrons and holes within the 1Σ′ feature. At the shortest t, the breadth of the 1Σ′ feature, ∼55 meV, is dictated by hole occupancy in the VB2/3 states. Within ∼2 ps, the occupancy signals become dominated by the electrons in the $1\Sigma_e'$ state, and the breadth of the 1Σ′ feature increases to ∼75 meV.

The $\Delta E_{Occ}(t)$ values obtained for all of the occupancy features in the $\Delta Abs_{Occ}(E, t)$ spectra collected with E_{exc} = 2.75 eV are plotted in Figure 6b. Recall, the occupancy features are only present when there are carriers in the quantum-confinement states associated with each feature. The energetic differences between the $\Delta E_{Occ}(t)$ values and the universal shift, 13 meV, obtained when extracting the $\Delta Abs_{Occ}(E, t)$ spectra from the $\Delta Abs_{TA}(E, t)$ spectra are attributed to additional QSR caused by the occupancy of charge carriers in any of the excited quantum-confinement states. These features are significantly weaker than the 1Σ′ features, due in large part to the smaller number of electrons and holes within these excited-states at any t. The largest $\Delta E_{Occ}(t)$ values are observed at the very short t, when the holes are quickly relaxing to the band edge and the electrons are still highly excited. The features shift to lower energies within t = 0.3 to 0.5 ps, after which the $\Delta E_{Occ}(t)$ values remain approximately the same. The $\Delta E_{Occ}(t)$ values for the 1Δ′/2Σ′ and 1Φ′/2Π′/1Γ′ excited-state features are larger than those of the lower-energy 1Σ′, 1Σ*′, and 1Π′ features. These differences are observed for as long as there are occupancies in these higher-energy features, > 1.5 ps. Trends for the 1Π′ occupancy feature are difficult to generalize as systematic changes are not clear, but the $\Delta E_{Occ}(t)$ values remain between those of the lower- and higher-energy features. The perturbations of the electron density created by the photoexcitation results in the largest QSR for the higher-energy quantum-confinement states.

The $\Delta E_{Occ}(t)$ values and spectral breadths of the occupancy features obtained with E_{exc} = 2.26 eV, Figure S14 and Figure S15, have similar characteristics as those measured with E_{exc} = 2.75 eV. There are subtle, justifiable differences between the data sets. The lower excitation energy results in the electrons and holes being prepared with less excess kinetic energies. As a result, the time required for the carriers, especially the electrons, to reach the band edge is less than when exciting with E_{exc} = 2.75 eV. The lower excitation energy also likely results in a smaller perturbation of the electron density in the QWs, and QSR that is initially smaller and closer to the long-time values. The observation of the 1Σ′-VB−1′ occupancy feature enables the relative amounts of QSR in VB′ and VB−1′ to be estimated. The average $\Delta E_{Occ}(t)$ values of the 1Σ′ feature at long t are 19(2) meV and 20(3) meV for excitation with E_{exc} = 2.75 eV and E_{exc} = 2.26 eV. The $\Delta E_{Occ}(t)$ values of the 1Σ′-VB−1′ feature, which we assign to be associated with transitions between the same quantum-confinement states as 1Σ′, are 30(4) meV and 34(4) meV for the two excitation energies. This suggests the degree of QSR in the lowest-lying quantum-confinement states within the VB−1 band is ∼1.5× to ∼1.7× greater than in the comparable states in the VB.

In summary, the QSR model was successfully applied to TA data collected on as-synthesized CdTe QWs (Φ_{PL} = 0.20(3)%). The occupancy spectra extracted contain details of the energetics and populations of charge carriers within the quantum-confinement states in the CB and VB. Time-

https://dx.doi.org/10.1021/acs.jpclett.0c01326
J. Phys. Chem. Lett. 2020, 11, 4901−4910

dependent occupancy profiles were obtained for each of the features to quantify the time scales for the relaxation of the charge carriers after initial excitation. Analyses of the spectral features and temporal profiles revealed separate time scales for the electrons and holes to reach the states near the band edge. Holes were determined to relax within the instrument resolution of the TA measurements, ~200 fs, while electrons relaxed slower, ~0.6 and ~0.7 eV ps^{-1} for excitation with E_{exc} = 2.75 and 2.26 eV, respectively. These electron relaxation rates are consistent with previously reported values for phonon scattering in bulk CdSe,[53] as opposed to two-body Auger relaxation. In general, the temporal profiles of higher-energy occupancy features were also consistent with the rapid relaxation of charge carriers through the manifold of high-energy states after initial excitation. Analyses of state-dependent relaxation within this manifold, however, were likely complicated by the numerous transitions underlying each of the occupancy features and competing nonradiative pathways that can occur at each step. The QSR model also allowed for the quantification of the energetic shifting of the quantum-confinement features within the Abs(E) spectrum. For both excitation energies used, a universal shift of ~13 meV to lower energy was determined at longer times when carriers occupy quantum-confinement states near the band edge. Additional energetic shifting for all of the features was observed at earlier times. In general, the higher-energy features shift by larger amounts than the lower features.

■ ASSOCIATED CONTENT

Supporting Information

The Supporting Information is available free of charge at https://pubs.acs.org/doi/10.1021/acs.jpclett.0c01326.

Details of the synthesis of the CdTe QWs, steady-state optical spectroscopy, quantum-confinement state and transition strength calculations, transient absorption measurements, extraction of occupancy contributions using the QSR model, exponential fitting of carrier occupancies, comparison of TA transient profiles with occupancy profiles, and additional data and figures are included (PDF).

■ AUTHOR INFORMATION

Corresponding Author

Richard A. Loomis − *Department of Chemistry and Institute of Materials Science and Engineering, Washington University in Saint Louis, Saint Louis, Missouri 63130, United States;* orcid.org/0000-0002-3172-6336; Email: loomis@wustl.edu

Authors

William M. Sanderson − *Department of Chemistry and Institute of Materials Science and Engineering, Washington University in Saint Louis, Saint Louis, Missouri 63130, United States;* orcid.org/0000-0001-5346-1730

Fudong Wang − *Department of Chemistry and Institute of Materials Science and Engineering, Washington University in Saint Louis, Saint Louis, Missouri 63130, United States;* orcid.org/0000-0003-2914-1360

Joshua Schrier − *Department of Chemistry, Fordham University, The Bronx, New York 10458, United States;* orcid.org/0000-0002-2071-1657

William E. Buhro − *Department of Chemistry and Institute of Materials Science and Engineering, Washington University in Saint Louis, Saint Louis, Missouri 63130, United States;* orcid.org/0000-0002-7622-4145

Complete contact information is available at: https://pubs.acs.org/10.1021/acs.jpclett.0c01326

Notes

The authors declare no competing financial interest.

■ ACKNOWLEDGMENTS

This work was supported by the NSF under Grants DMR-1611149 and DMR-1905751 (R.A.L.) and CHE-1607862 (W.E.B.). J.S. acknowledges the Henry Dreyfus Teacher-Scholar Award (TH-14-010). This research used resources of the National Energy Research Scientific Computing Center (NERSC), a U.S. Department of Energy Office of Science User Facility operated under Contract DE-AC02-05CH11231.

■ REFERENCES

(1) Kamat, P. V. Quantum Dot Solar Cells. Semiconductor Nanocrystals as Light Harvesters. *J. Phys. Chem. C* **2008**, *112*, 18737−18753.

(2) Krauss, T. D.; Wise, F. W. Coherent Acoustic Phonons in a Semiconductor Quantum Dot. *Phys. Rev. Lett.* **1997**, *79*, 5102−5105.

(3) Guyot-Sionnest, P.; Shim, M.; Matranga, C.; Hines, M. Intraband Relaxation in CdSe Quantum Dots. *Phys. Rev. B: Condens. Matter Mater. Phys.* **1999**, *60*, R2181.

(4) Wise, F. W. Lead Salt Quantum Dots: The Limit of Strong Quantum Confinement. *Acc. Chem. Res.* **2000**, *33*, 773−780.

(5) Sewall, S. L.; Cooney, R. R.; Anderson, K. E. H.; Dias, E. A.; Kambhampati, P. State-to-State Exciton Dynamics in Semiconductor Quantum Dots. *Phys. Rev. B: Condens. Matter Mater. Phys.* **2006**, *74*, 235328.

(6) Son, D. H.; Wittenberg, J. S.; Banin, U.; Alivisatos, A. P. Second Harmonic Generation and Confined Acoustic Phonons in Highly Excited Semiconductor Nanocrystals. *J. Phys. Chem. B* **2006**, *110*, 19884−19890.

(7) Sagar, D. M.; Cooney, R. R.; Sewall, S. L.; Kambhampati, P. State-Resolved Exciton-Phonon Couplings in CdSe Semiconductor Quantum Dots. *J. Phys. Chem. C* **2008**, *112*, 9124−9127.

(8) Hendry, E.; Pijpers, J.; Bonn, M. Ultrafast Intraband Relaxation in Colloidal Quantum Dots. In *Proc. of SPIE, Ultrafast Phenomena in Semiconducgtors and Nanostructure Materials XII*, Sept 15−19 2008; IEEE: 2008; pp 1−3.

(9) Huxter, V. M.; Lee, A.; Lo, S. S.; Scholes, G. D. CdSe Nanoparticle Elasticity and Surface Energy. *Nano Lett.* **2009**, *9*, 405−409.

(10) Klimov, V. I. Properties of Multiexcitons in Semiconductor Nanocrystals. *Annu. Rev. Phys. Chem.* **2007**, *58*, 635−673.

(11) Logunov, S.; Green, T.; Marguet, S.; El-Sayed, M. A. Interfacial Carriers Dynamics of CdS Nanoparticles. *J. Phys. Chem. A* **1998**, *102*, 5652−5658.

(12) Burda, C.; Green, T. C.; Link, S.; El-Sayed, M. A. Electron Shuttling across the Interface of CdSe Nanoparticles Monitored by Femtosecond Laser Spectroscopy. *J. Phys. Chem. B* **1999**, *103*, 1783−1788.

(13) Aldana, J.; Wang, Y. A.; Peng, X. Photochemical Instability of CdSe Nanocrystals Coated by Hydrophilic Thiols. *J. Am. Chem. Soc.* **2001**, *123*, 8844−8850.

(14) Nazzal, A. Y.; Wang, X.; Qu, L.; Yu, W.; Wang, Y.; Peng, X.; Xiao, M. Environmental Effects on Photoluminescence of Highly Luminescent CdSe and CdSe/ZnS Core/Shell Nanocrystals in Polymer Thin Films. *J. Phys. Chem. B* **2004**, *108*, 5507−5515.

(15) Wuister, S. F.; de Mello Donega, C.; Meijerink, A. Influence of Thiol Capping on the Exciton Luminescence and Decay Kinetics of

CdTe and CdSe Quantum Dots. *J. Phys. Chem. B* **2004**, *108*, 17393−17397.
(16) Akamatsu, K.; Tsuruoka, T.; Nawafune, H. Band Gap Engineering of CdTe Nanocrystals through Chemical Surface Modification. *J. Am. Chem. Soc.* **2005**, *127*, 1634−1635.
(17) Achtstein, A. W.; Scott, R.; Kickhöfel, S.; Jagsch, S. T.; Christodoulou, S.; Bertrand, G. H. V.; Prudnikau, A. V.; Antanovich, A.; Artemyev, M.; Moreels, I.; Schliwa, A.; Woggon, U. *P*-State Luminescence in CdSe Nanoplatelets: Role of Lateral Confinement and a Longitudinal Optical Phonon Bottleneck. *Phys. Rev. Lett.* **2016**, *116*, 116802.
(18) Peterson, M. D.; Cass, L. C.; Harris, R. D.; Edme, K.; Sung, K.; Weiss, E. A. The Role of Ligands in Determining the Exciton Relaxation Dynamics in Semiconductor Quantum Dots. *Annu. Rev. Phys. Chem.* **2014**, *65*, 317−339.
(19) Guyot-Sionnest, P.; Wehrenberg, B.; Yu, D. Intraband Relaxation in CdSe Nanocrystals and the Strong Influence of the Surface Ligands. *J. Chem. Phys.* **2005**, *123*, 074709.
(20) Harris, R. D.; Bettis Homan, S.; Kodaimati, M.; He, C.; Nepomnyashchii, A. B.; Swenson, N. K.; Lian, S.; Calzada, R.; Weiss, E. A. Electronic Processes within Quantum Dot-Molecule Complexes. *Chem. Rev.* **2016**, *116*, 12865−12919.
(21) Singh, S.; Tomar, R.; ten Brinck, S.; De Roo, J.; Geiregat, P.; Martins, J. C.; Infante, I.; Hens, Z. Colloidal CdSe Nanoplatelets, a Model for Surface Chemistry/Optoelectronic Property Relations in Semiconductor Nanocrystals. *J. Am. Chem. Soc.* **2018**, *140*, 13292−13300.
(22) Olshansky, J. H.; Ding, T. X.; Lee, Y. V.; Leone, S. R.; Alivisatos, A. P. Hole Transfer from Photoexcited Quantum Dots: The Relationship between Driving Force and Rate. *J. Am. Chem. Soc.* **2015**, *137*, 15567−15575.
(23) Diroll, B. T.; Fedin, I.; Darancet, P.; Talapin, D. V.; Schaller, R. D. Surface-Area-Dependent Electron Transfer between Isoenergetic 2D Quantum Wells and a Molecular Acceptor. *J. Am. Chem. Soc.* **2016**, *138*, 11109−11112.
(24) Cassette, E.; Pedetti, S.; Mahler, B.; Ithurria, S.; Dubertret, B.; Scholes, G. D. Ultrafast Exciton Dynamics in 2D in-Plane Hetero-Nanostructures: Delocalization and Charge Transfer. *Phys. Chem. Chem. Phys.* **2017**, *19*, 8373−8379.
(25) Hoheisel, W.; Colvin, V. L.; Johnson, C. S.; Alivisatos, A. P. Threshold for Quasicontinuum Absorption and Reduced Luminescence Efficiency in CdSe Nanocrystals. *J. Chem. Phys.* **1994**, *101*, 8455−8460.
(26) Hoy, J.; Morrison, P. J.; Steinberg, L. K.; Buhro, W. E.; Loomis, R. A. Excitation Energy Dependence of the Photoluminescence Quantum Yields of Core and Core/Shell Quantum Dots. *J. Phys. Chem. Lett.* **2013**, *4*, 2053−2060.
(27) Geißler, D.; Würth, C.; Wolter, C.; Weller, H.; Resch-Genger, U. Excitation Wavelength Dependence of the Photoluminescence Quantum Yield and Decay Behavior of CdSe/CdS Quantum Dot/Quantum Rods with Different Aspect Ratios. *Phys. Chem. Chem. Phys.* **2017**, *19*, 12509−12516.
(28) Martynenko, I. V.; Baimuratov, A. S.; Osipova, V. A.; Kuznetsova, V. A.; Purcell-Milton, F.; Rukhlenko, I. D.; Fedorov, A. V.; Gun'ko, Y. K.; Resch-Genger, U.; Baranov, A. V. Excitation Energy Dependence of the Photoluminescence Quantum Yield of Core/Shell CdSe/CdS Quantum Dots and Correlation with Circular Dichroism. *Chem. Mater.* **2018**, *30*, 465−471.
(29) Li, B.; Brosseau, P. J.; Strandell, D. P.; Mack, T. G.; Kambhampati, P. Photophysical Action Spectra of Emission from Semiconductor Nanocrystals Reveal Violations to the Vavilov Rule Behavior from Hot Carrier Effects. *J. Phys. Chem. C* **2019**, *123*, 5092−5098.
(30) Roy, D.; Das, A.; De, C. K.; Mandal, S.; Bangal, P. R.; Mandal, P. K. Why Does the Photoluminescence Efficiency Depend on Excitation Energy in Case of a Quantum Dot? A Case Study of CdSe-Based Core/Alloy Shell/Shell Quantum Dots Employing Ultrafast Pump−Probe Spectroscopy and Single Particle Spectroscopy. *J. Phys. Chem. C* **2019**, *123*, 6922−6933.
(31) Klimov, V. I.; McBranch, D. W.; Leatherdale, C. A.; Bawendi, M. G. Electron and Hole Relaxation Pathways in Semiconductor Quantum Dots. *Phys. Rev. B: Condens. Matter Mater. Phys.* **1999**, *60*, 13740−13749.
(32) Lo, S. S.; Major, T. A.; Petchsang, N.; Huang, L. B.; Kuno, M.; Hartland, G. V. CdTe Nanowires Studied by Transient Absorption Microscopy. *EPJ Web Conf.* **2013**, *41*, 04032.
(33) Carey, C. R.; Yu, Y.; Kuno, M.; Hartland, G. V. Ultrafast Transient Absorption Measurements of Charge Carrier Dynamics in Single II-VI Nanowires. *J. Phys. Chem. C* **2009**, *113*, 19077−19081.
(34) Dong, S.; Pal, S.; Lian, J.; Chan, Y.; Prezhdo, O. V.; Loh, Z.-H. Sub-Picosecond Auger-Mediated Hole-Trapping Dynamics in Colloidal CdSe/CdS Core/Shell Nanoplatelets. *ACS Nano* **2016**, *10*, 9370−9378.
(35) Knowles, K. E.; McArthur, E. A.; Weiss, E. A. A Multi-Timescale Map of Radiative and Nonradiative Decay Pathways for Excitons in CdSe Quantum Dots. *ACS Nano* **2011**, *5*, 2026−2035.
(36) Li, Q.; Lian, T. A Model for Optical Gain in Colloidal Nanoplatelets. *Chem. Sci.* **2018**, *9*, 728−734.
(37) McArthur, E. A.; Morris-Cohen, A. J.; Knowles, K. E.; Weiss, E. A. Charge Carrier Resolved Relaxation of the First Excitonic State in CdSe Quantum Dots Probed with near-Infrared Transient Absorption Spectroscopy. *J. Phys. Chem. B* **2010**, *114*, 14514−14520.
(38) Mooney, J.; Krause, M. M.; Kambhampati, P. Connecting the Dots: The Kinetics and Thermodynamics of Hot, Cold, and Surface-Trapped Excitons in Semiconductor Nanocrystals. *J. Phys. Chem. C* **2014**, *118*, 7730−7739.
(39) Morgan, D. P.; Maddux, C. J. A.; Kelley, D. F. Transient Absorption Spectroscopy of CdSe Nanoplatelets. *J. Phys. Chem. C* **2018**, *122*, 23772−23779.
(40) Puthussery, J.; Lan, A. D.; Kosel, T. H.; Kuno, M. Band-Filling of Solution-Synthesized CdS Nanowires. *ACS Nano* **2008**, *2*, 357−367.
(41) Robel, I.; Bunker, B. A.; Kamat, P. V.; Kuno, M. Exciton Recombination Dynamics in CdSe Nanowires: Bimolecular to Three-Carrier Auger Kinetics. *Nano Lett.* **2006**, *6*, 1344−1349.
(42) Yan, Y.; Chen, G.; Van Patten, P. G. Ultrafast Exciton Dynamics in CdTe Nanocrystals and Core/Shell CdTe/CdS Nanocrystals. *J. Phys. Chem. C* **2011**, *115*, 22717−22728.
(43) Sanderson, W. M.; Schrier, J.; Loomis, R. A. Photo-Induced State Shifting in 1D Semiconductor Quantum Wires. submitted to *J. Phys. Chem. C* **2020**.
(44) Liu, Y.-H.; Wang, F.; Hoy, J.; Wayman, V. L.; Steinberg, L. K.; Loomis, R. A.; Buhro, W. E. Bright Core−Shell Semiconductor Quantum Wires. *J. Am. Chem. Soc.* **2012**, *134*, 18797−18803.
(45) Sun, J. W.; Buhro, W. E.; Wang, L. W.; Schrier, J. Electronic Structure and Spectroscopy of Cadmium Telluride Quantum Wires. *Nano Lett.* **2008**, *8*, 2913−2919.
(46) Chelikowsky, J. R.; Cohen, M. L. Nonlocal Pseudopotential Calculations for the Electronic Structure of Eleven Diamond and Zinc-Blende Semiconductors. *Phys. Rev. B* **1976**, *14*, 556−582.
(47) Sanderson, W. M.; Wang, F.; Buhro, W. E.; Loomis, R. A. Long-Lived 1D Excitons in Bright CdTe Quantum Wires. *J. Phys. Chem. C* **2019**, *123*, 3144−3151.
(48) Sanderson, W. M.; Hoy, J.; Morrison, C.; Wang, F.; Wang, Y.; Morrison, P. J.; Buhro, W. E.; Loomis, R. A. Excitation Energy Dependence of Photoluminescence Quantum Yields of Semiconductor Nanoparticles with Varying Dimensionalities. *J. Phys. Chem. Lett.* **2020**, *11*, 3249−3256.
(49) Rabouw, F. T.; Kamp, M.; van Dijk-Moes, R. J. A.; Gamelin, D. R.; Koenderink, A. F.; Meijerink, A.; Vanmaekelbergh, D. Delayed Exciton Emission and Its Relation to Blinking in CdSe Quantum Dots. *Nano Lett.* **2015**, *15*, 7718−7725.
(50) Rabouw, F. T.; van der Bok, J. C.; Spinicelli, P.; Mahler, B.; Nasilowski, M.; Pedetti, S.; Dubertret, B.; Vanmaekelbergh, D. Temporary Charge Carrier Separation Dominates the Photoluminescence Decay Dynamics of Colloidal CdSe Nanoplatelets. *Nano Lett.* **2016**, *16*, 2047−2053.

https://dx.doi.org/10.1021/acs.jpclett.0c01326
J. Phys. Chem. Lett. 2020, 11, 4901−4910

(51) Whitham, P. J.; Marchioro, A.; Knowles, K. E.; Kilburn, T. B.; Reid, P. J.; Gamelin, D. R. Single-Particle Photoluminescence Spectra, Blinking, and Delayed Luminescence of Colloidal $CuInS_2$ Nanocrystals. *J. Phys. Chem. C* **2016**, *120*, 17136−17142.
(52) Marchioro, A.; Whitham, P. J.; Nelson, H. D.; De Siena, M. C.; Knowles, K. E.; Polinger, V. Z.; Reid, P. J.; Gamelin, D. R. Strong Dependence of Quantum-Dot Delayed Luminescence on Excitation Pulse Width. *J. Phys. Chem. Lett.* **2017**, *8*, 3997−4003.
(53) Klimov, V. I.; McBranch, D. W. Femtosecond 1*P*-to-1*S* Electron Relaxation in Strongly Confined Semiconductor Nanocrystals. *Phys. Rev. Lett.* **1998**, *80*, 4028−4031.

https://dx.doi.org/10.1021/acs.jpclett.0c01326
J. Phys. Chem. Lett. 2020, 11, 4901−4910